# Fluoride-Mediated Desulfonylative Intramolecular Cyclization to Fused and Bridged Bicyclic Compounds: A Complex Mechanism

Michelle Bezanson, Anna Tomberg, and Nicolas Moitessier*

Department of Chemistry, McGill University, 801 Sherbrooke Street West, Montreal, Quebec, Canada H3A 0B8

S *Supporting Information*

ABSTRACT: We previously reported the synthesis of polysubstituted chiral oxazepanes in three steps from commercially available starting materials. The unexpected reaction of one of these 1,4-oxazepanes in the presence of TBAF provided a 4-oxa-1-azabicyclo[4.1.0]heptane core. This unusual process significantly increased the complexity of the molecular scaffold by introducing a bicyclic core. Surprisingly, the generated bicyclic structure featuring three stereocenters was a mixture of enantiomers with no other diastereomers observed. These striking experimental observations deserved further investigations. A combination of experimental and computational investigations unveiled a complex diastereoselective mechanism. Mechanistic rationale is presented for this observed rearrangement.
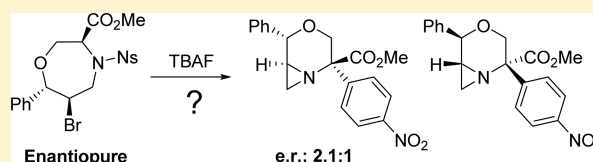
INTRODUCTION

One powerful method of introducing molecular complexity is through intramolecular rearrangements of heterocyclic compounds, with perhaps some of the best examples being in the context of diversity-oriented synthesis.[1,2] Many of these methods are metal-catalyzed, decreasing the applicability of such reactions in green processes or significantly increasing the associated costs.[3−6] Over the past century, several very different rearrangements were discovered, such as the very well-known Claisen and Wittig rearrangements of allylic systems, the Brook rearrangement of α-silyl carbinols,[7] and the Wolff rearrangement, to name a few.[8] Other rearrangements on aromatic molecules are also well established, such as the Snieckus−Fries rearrangement.[9,10] Over the years, other complex rearrangements were also discovered from judiciously designed experiments leading to unexpected results.[11,12]

In recent years, we reported the design, development, and use of a number of chiral molecular scaffolds. Among those are bicyclic dipeptide mimetics,[13] carbohydrates,[14] and polysubstituted oxazepanes and morpholines.[15] The latter were prepared in three steps from commercially available starting materials in good to excellent stereoselectivity and regioselectivity (Figure 1). To use these scaffolds, the two protecting groups (methyl ester and nosyl) should be removed to release the two functiona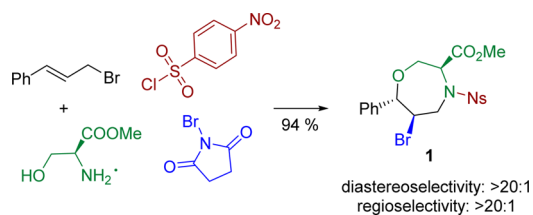lizable anchors (carboxylic acid and secondary amine). In an attempt to remove the sulfonamide protecting group on oxazepane **1** using tetrabutylammonium fluoride (TBAF), we observed full conversion to a nonracemic mixture of enantiomeric products.

Herein, we report a unique fluoride-mediated rearrangement of 1,4-oxazepanes and morpholines together with an extensive mechanistic study, revealing a complex series of reactions.

RESULTS AND DISCUSSION

Characterization. NMR characterization indicated that the para-substituted phenyl group of the nosyl protecting group was still present with a significant upfield shift of the aromatic protons. Additional investigations by mass spectrometry (MS) suggested loss of SO_2 and led us to consider an intramolecular rearrangement. Extensive NMR studies as well as X-ray crystallography confirmed the structure of the obtained product to be **2** (Figure 2). Although oxazepane **1** was enantiopure, the crystal structure of **2** was of the racemic compound, and chiral HPLC showed that the reaction proceeded with 36% ee (see Supporting Information).

Figure 2. Fluoride-mediated intramolecular rearrangement of **1**. Ellipsoids shown at the 50% probability level. The crystal structure is of (±)-**2** (the enantiomer shown will be referred to as **2a**; the enantiomer not shown will be referred to as **2b**).
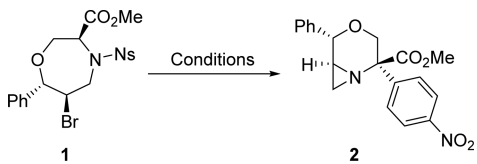

Figure 1. Complexity from simple building blocks.

Overall, the process included desulfurization, migration of a *para*-nitrophenyl group, intramolecular cyclization to an aziridine, and racemization. This uncommon process may represent a powerful method for introducing significant complexity in very few steps, including bridged and fused ring systems; thus, it deserved to be further investigated, and its mechanism should be elucidated.

Probing the Reaction Conditions. To understand the mechanism, we examined a variety of conditions (Table 1).

Table 1. Reaction Condition Evaluation

entry	reagent[a]	conversion (%)[b]
1	TBAF[c]	100
2	TBACl	0
3	TBAB	0
4	TBAI	0
5	pyridinium fluoride	0
6	NaF + 15-crown-5	0
7	K$_2$CO$_3$	0
8	NEt$_3$	<5
9	KO^{t}Bu + 18-crown-6	complex mixture
10	NaOH	0[d]
11	AgOTf	0
12	0.2 eq. TBAF	35
13	1 eq. TBAF	38
14	reflux	complex mixture
15[e]	−78 °C	100
16	[1] = 0.20 M	100
17	solid TBAF[f]	100
18	solid TBAF[f], MeOH	0
19	solid TBAF[f], toluene	100

[a]Reaction conditions: [1] = 0.02 M, reagent (5 equiv), THF, rt. [b]Determined by HPLC. [c]TBAF is a 1 M solution in THF. [d]Starting material is completely consumed. [e]An intermediate was observed in the HPLC trace of this crude mixture; however, it converted completely to the expected product within an hour. [f]Solid TBAF is tetrabutylammonium fluoride hydrate.

Surprisingly, TBAF was the only additive that initiated this unique rearrangement efficiently. It is known that TBAF can act as a strong base and is able to initiate amides and carbamates to undergo intramolecular cyclization.[16,17] Additionally, there have been a few reports of aryl migration of nosyl protecting groups accompanied by extrusion of sulfur dioxide under basic conditions.[18,19] In light of this known reactivity, we first reasoned that TBAF was acting as a base to initiate the reaction. The presence of the large nosyl group close to the enolizable proton may be preventing larger anions like chloride, bromide, and iodide from initiating the reaction. Alternatively, these halides may not be basic enough to promote the reaction (Table 1, entries 2−4). The lack of reactivity observed when pyridinium fluoride was employed was thought to arise from the stronger ion pair formed compared to TBAF reducing the reactivity of fluoride (Table 1, entry 5). However, when NaF was employed in conjunction with 15-crown-5 ether, no reaction was observed, indicating that the availability of the

fluoride ion may not be the issue, unless an ion pair is retained with the crown ether complex (Table 1, entry 6).

Bases other than TBAF such as K$_2$CO$_3$ and NEt$_3$ either did not initiate this reaction or did so with low conversion (Table 1, entries 7 and 8). This observation ruled out the possibility that NBu$_3$, a decomposition product of TBAF, played any substantial role. This prompted us to question if TBAF was indeed acting as a simple base and to look at stronger bases. When KO^{t}Bu was employed, the starting material was completely consumed, but only a complex mixture was obtained and no rearranged product was observed (Table 1, entry 9), indicating that the starting material and/or the products were not stable under strongly basic conditions. Similarly, when we employed NaOH, the starting material was again completely consumed, but no rearranged product was obtained, indicating that any basic hydroxides present in the commercial TBAF were not responsible for the observed reactivity (Table 1, entry 10). We also investigated the use of Lewis acids as activating agents to increase reactivity, yet when AgOTf was employed, only starting material was recovered (Table 1, entry 11).

An excess of TBAF was required to drive the reaction to completion; however, the similar conversions observed when employing substoichiometric or 1 equiv of TBAF did not allow us to rule out a catalytic mechanism (Table 1, entries 12 and 13).

We next examined the effect of temperature on the reaction (Table 1, entries 14 and 15). Interestingly, at −78 °C, a short half-life intermediate was observed by monitoring the reaction by HPLC. This intermediate converted completely to **2** over time. At elevated temperatures, only decomposition was observed.

The effect of the concentration of the starting material on the reaction seemed to be unimportant as increasing the concentration by up to an order of magnitude had little effect on the reaction (Table 1, entry 16). Lastly, we examined the effect of the solvent on the reaction. The TBAF used under the standard conditions was a 1 M solution in THF. To vary the solvents, solid TBAF hydrate was also assessed. This was tested first in THF to ensure that the outcome was similar to that observed when TBAF solution was employed (Table 1, entry 17). At this stage, we could assume that solid TBAF hydrate was an acceptable substitute for TBAF solution. Performing the reaction in toluene gave similar results to those using THF. However, only starting material was isolated when methanol was employed (Table 1, entries 18 and 19). This observation was consistent with TBAF acting as a weaker base in protic solvents such as methanol.

Control Experiments. We strategically chose a variety of substrates; this was done not to show how widely applicable this chemistry is but, rather, to glean as much mechanistic detail as possible. The selected set of substrates and the observed products are presented in Table 2.

As the bromine atom acts as a leaving group, substituting it with iodine should not affect the outcome. Unsurprisingly, the 6-iodo derivative (**3a**) gave the same product as **1** (Table 2, entry 2).

When an analogous morpholine substrate (**3b**) was subjected to the reaction conditions, the major product isolated was fused bicycle **4b** (Table 2, entry 3). The structure of the product suggested that formation of an enolate occurred, followed by displacement of the bromide (Figure 3). This is additional evidence that fluoride is acting as a base.

Table 2. Control Experiments

Entry	Compound	Starting Material	% Conversion[a] (Isolated Yield)	Product(s) Isolated
1	**1**		> 99 (46)	**2**, 36 %ee
2	**3a**		> 99[b]	**2**
3	**3b**		> 99 (27)	**4b**
4	**3c**		–[c]	**4c**
5	**3d**		> 99 (69)	**4d**
6	**3e**		–	Complex mixture
7	**3f**		> 99	**4fa** **4fb** **4fc** **4fd**
8	**3g**		> 99 (69)	**4g**
9[d]	**3h**		> 99	**4ha** **4hb** **4g** **4hd**
10[e]	**3i**		> 99 (21)	**4i**
11[e]	**3j**		> 99 (22)	**4j**

[a]Determined by HPLC; >99% indicates that no remaining starting material could be detected. [b]**3a′**, with the opposite stereochemistry at C6 and C7, also gave **2** exclusively with full conversion; no % ee was measured for either reaction. [c]HPLC signals for starting material overlapped with those of the products, so conversion could not be reported; no starting material was recovered. [d]Products shown were assumed based on the proposed mechanism and isolation of **4hb** proving to be the enantiomer of **4fb**. [e]Enantiomeric excess was not determined.
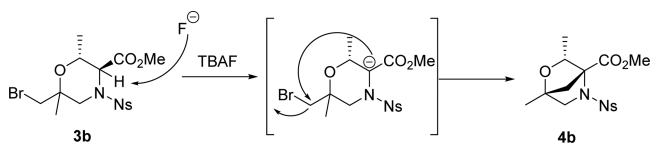
Figure 3. Mechanism for the formation of **4b**.

We hypothesized that in the absence of an enolizable proton no rearrangement would occur (Table 2, entry 4), and we carried out the reaction with the 3-unsubstituted derivative **3c**. Only the elimination product **4c** was observed. Importantly, no rearranged bicycle product was observed, indicating that an enolizable proton is required. Together with the previous observation with the morpholine substrate (Table 2, entry 3) and literature precedents,[19] this piece of information strongly suggests that an enolate is involved in the mechanism.

To rationalize the isomerization of the benzylic position, we imagined that a possible mechanistic pathway might involve participation of the benzylic proton. To examine this potential mechanism, we replaced the phenyl group by an achiral gem dimethyl moiety in **3d** (Table 2, entry 5). The only product observed was **4d**, indicating that the benzylic proton was not necessary for the reaction to proceed and therefore unlikely to be involved in the mechanism. However, the presence of a single stereoisomer does not provide any information about the role of this hydrogen in the isomerization of the product as this could indicate a highly stereoselective isomerization or no isomerization.

Next, we wanted to examine the electronic effects of the sulfonamide group on the observed reactivity. We hypothesized that migration of the aryl group occurred from attack of an enolate at C3 onto the ipso carbon of the nosyl protecting group. We thought that the ipso carbon of a tosyl protecting group (**3e**) would be less electrophilic. In addition, the lower electron-withdrawing abilities of the tosyl relative to nosyl may also have an effect on the acidity of the C3 proton, making the enolate more difficult to form and possibly even shutting down the reaction. In light of these hypotheses, we were pleased to see that, while a reaction indeed occurred with the tosylated derivative, the reaction resulted in a very complex mixture that did not seem to follow the same trends as the reactivity of the nosylated derivative (Table 2, entry 6). This observation is also consistent with previous observations on proline esters where moving from nosyl to tosyl shut down the migration reaction (Figure 4).[19]
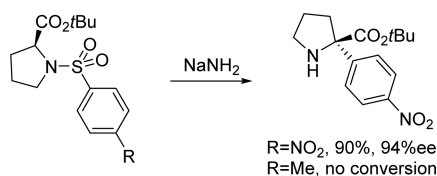

Figure 4. Migration of *para*-nitrophenyl in nosyl-protected proline ester reported previously.[19]

While the migration of aryl sulfonamide proline esters is documented to occur under strongly basic conditions (Figure 4), the partial racemization that we observed was puzzling. Mechanistically, the partial racemization that we observed for the formation of **2** indicated that all three of the stereocenters on the molecule must participate in the mechanism. We thought that the addition of another stereocenter would give

information about the involvement of that center in the mechanism; additionally, we wanted to examine the effect that this additional stereocenter had on the selectivity of the reaction. For this purpose, we looked at threonine analogue **3f** and isolated not a single compound as we did with **1** but, in fact, a mixture of several compounds (Table 2, entry 7). After tedious purification and characterization, we were able to assign structures as **4fa**, **4fb**, **4fc**, and **4fd**. Interestingly, **4fa** was very difficult to isolate reproducibly. Despite this poor stability, we were able to get a crystal structure of **4fa** to confirm the structure we had initially assigned by NMR (Figure 5). We
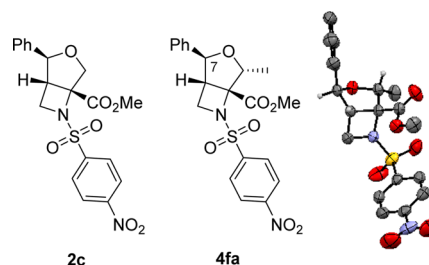

Figure 5. Assigned structure of **2c** based on a comparison of its NMR spectrum with that of **4fa**. Ellipsoids are shown at the 50% probability level.

previously mentioned a short half-life intermediate observed at low temperature when reacting **1**. At this point, we assigned the structure of the intermediate isolated at low temperatures mentioned above (Table 1, entry 15) to be **2c** based on a comparison of the ^{1}H NMR spectrum with that of **4fa**. It is important to note that the stereochemistry at the C7 phenyl group had inverted relative to the stereochemistry of the starting material. As this was the only product isolated from the reaction that had the nosyl protecting group intact, this was strong evidence that the stereochemistry at C7 was affected prior to migration of the *para*-nitrophenyl group.

Extensive NMR studies suggested that the structures of **4fb** and **4fc** were diastereomeric. When we strategically designed this experiment, we proposed the introduction of an additional stereocenter relative to **2** (i.e., additional methyl from **1** to **3f**) to determine if that carbon atom was also involved in the mechanism. The formation of diastereomers differing in all but this center indicated that the C2 center was not involved in the isomerization mechanism. There was an obvious matched/mismatched effect happening, however, as **4fb** was significantly favored over **4fc**.

Epoxide **4fd** represented an interesting scaffold and exemplified how fascinating this reaction was mechanistically. Two possible mechanisms for the formation of **4fd** are presented in Figure 6. With threonine, the additional methyl enables the formation of an epoxide after migration of the *para*-nitrophenyl, with elimination/ring opening taking place on the threonine side chain methyl group to produce **4fd** after loss of SO_2 (Figure 6, pathway 1). Alternatively, fluoride abstraction of the enolizable proton may lead to a retro-Michael addition, and the generated alkoxide then concertedly displaces the bromide to form epoxide **4fd** (Figure 6, pathway 2). Assistance of the sulfonamide oxygen is possible and has not been investigated further.

When comparing the stereochemical outcome of the reactions with serine derivative **1** and threonine derivative **3f**, it was clear that the additional stereogenic center was
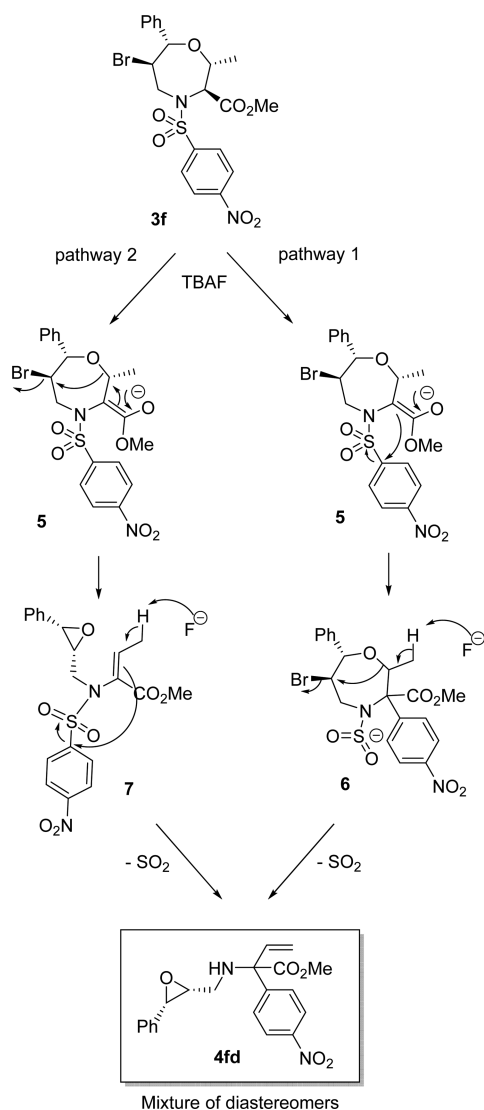
Figure 6. Tentative mechanisms for the formation of **4fd**.

modulating the stereoselectivity. We reasoned that inverting the C2 stereochemistry, which was responsible for the matched/ mismatched behavior, may invert the stereopreference. To probe this hypothesis, we varied the stereochemistry at C6 and C7 using *allo*-threonine-derived starting oxazepane. As predicted, when reacting **3g**, the C2 epimer of **3f**, only one product was isolated, **4g** (Table 2, entry 8). Once more the relative stereochemistry among the three isomerizable centers was identical to that of **2** and was unique as no diastereomers were observed. When reacting **3h**, which was diastereomeric with **3f** at C2, C6, and C7, the HPLC trace was identical to the crude of **3f**. This indicated that the transition states of the reaction of **3h** were enantiomeric with those from **3f** since the C2 stereocenter is not involved in the reaction (Table 2, entry 9). Indeed, isolation of the major compound from this reaction, **4hb**, showed an identical proton NMR as that of **4fb** together with an optical rotation measurement of the opposite sign, lending even further evidence toward this hypothesis.

As apparent in Table 2, the isolated yields are significantly lower than the conversions. These compounds were very difficult to isolate as pure products using flash chromatography and difficult to monitor by TLC. As this work is focused on the mechanism, we did not optimize the isolation procedures.

Proposed Mechanism. At this point, we point out that the proposal is still a tentative mechanism, although we believe that we have presented herein a reasonable suggestion that is supported by extensive computational investigations. The calculations were performed using DFT in THF implicit solvent (see the Supporting Information for details).

To account for the clean conversion of medium-sized ring derivative **1** into bicyclic molecule **2**, we undertook computational modeling of the reaction mechanism. With the substrate scope in hand, we had a wealth of information to consider when developing a proposed mechanism. One particularly significant observation was the isolation of **4fa**, which suggested that the inversion of stereochemistry at C7 occurs before migration of the *para*-nitrophenyl group. This inversion likely goes through an sp^2 intermediate, via either a carbocationic intermediate or an olefin intermediate.

To probe inversion of stereochemistry going through a carbocation, we analyzed computationally the formation of a carbon−oxygen bond (marked red in Figure 7). By computing
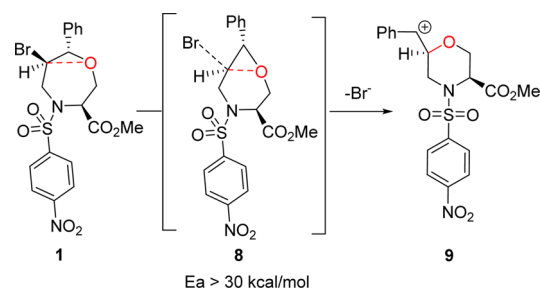

Figure 7. Formation of carbocation intermediate **9** from **1**.

the energies along the varying bond length between these two atoms, we estimated the energy barrier required for this step to be over 30 kcal/mol, which indicated that this pathway is unlikely.

The alternative way of inverting the stereochemistry at C7 is through an olefin formed through opening the seven-membered ring by an elimination reaction. This step required a specific conformation of the ring where the C6 proton oriented almost perfectly antiperiplanar to the ether oxygen, making elimination a favorable option (Figure 8).

This conformation (**1′**), stabilized by a fluoride anion and an HF molecule, was 3.1 kcal/mol lower in energy than compound **1** under otherwise identical conditions. An energy barrier of 14.9 kcal/mol was required to produce the open structure **10** (Figure 9) though an E2 mechanism from **1′**. The free rotation
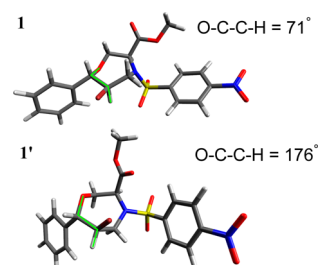

Figure 8. Compound **1**: conformation leading toward **2a** (top) and conformation with the C6 proton antiperiplanar to the ether oxygen, leading to elimination of bromine and, eventually, formation of **2b** (bottom).
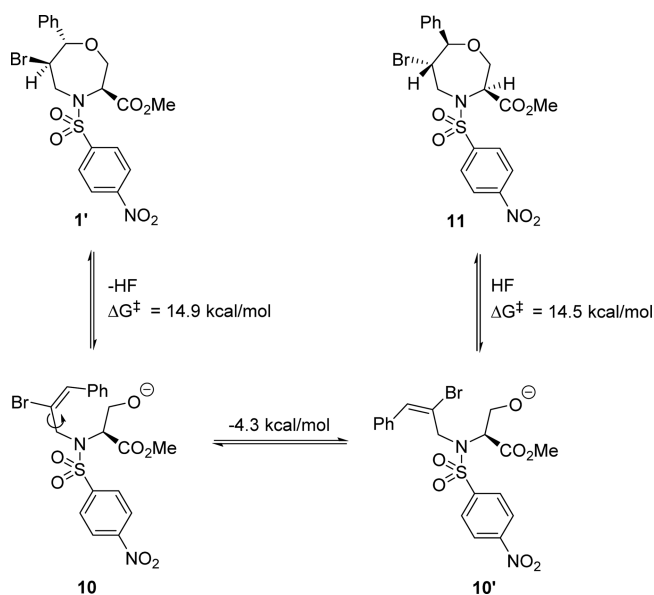
Figure 9. Ring opening of **1′** leading to the production of its diastereomer, **11**.

around the carbon−carbon bond to yield **10′** is energetically favorable by 4.3 kcal/mol, thereby allowing the substituents at C6 and C7 to invert relative to **1** once the ring closes to **11**. The two structures, **1** and **11**, have similar energies, with **11** being 0.9 kcal/mol lower.

It is worth noting that only one conformation of compound **1** possesses this antiperiplanar geometry and will undergo the elimination mechanism. Similarly, we suggest that this elimination becomes more or less favorable for other substrates such as threonine (**3f**) or *allo*-threonine (**3g,h**) based substrates depending on the energy associated with their conformations. This would account for the matched/mismatched effect that is observed, particularly between **3g** and **3h**.

The formation of this double bond conjugated with the phenyl ring as an explanation for the isomerization is in agreement with the single isomer (no isomerization) observed with substrates that either cannot form this double bond (**3i**; Table 2, entry 10) or would lead to a nonconjugated double bond (**3j**; Table 2, entry 11).

With a reasonable mechanism to give both stereoisomers at C7, we proposed the next step to be the formation of enantiomeric enolates **12a** and **12b** from **1** and **11**, respectively. An energy of activation of 1.3 and 4.9 kcal/mol was predicted, respectively (Figure 10). Thus, computation confirmed that enolization is possible and that the fluoride ion is basic enough in THF for this step to take place.

We investigated migration of the *para*-nitrophenyl as the next step in the mechanism. Since enolates **12a** and **12b** are enantiomeric, for simplicity, only **12a** will be discussed. The process for **12b** is the mirror image and will have identical energies. The formation of **13a** from **12a** (Figure 11) needed to
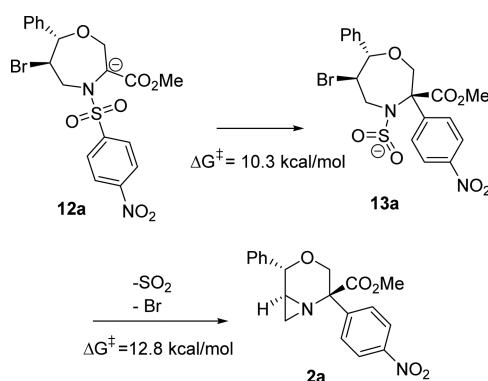

Figure 11. Formation of product **2a** from enolate **12a** (same for **2b** from **12b**).

overcome an energy barrier of 10.3 kcal/mol, going through a highly exergonic process. The last step connecting this pathway to the observed product **2a** was the loss of SO$_2$, ring contraction to form the aziridine, and displacement of bromide anion. This process has an energy of activation of 12.8 kcal/mol.

Keeping in mind that there could be other pathways to explain the formation of **2b**, we investigated other possibilities to produce this enantiomer. For example, **12a** could change conformations, prompting the nosyl on top of the neighboring −CO$_2$Me (**12a′**), which would allow the formation of **14** after the migration of *para*-nitrophenyl (Figure 12). Then, similarly to the process described in Figure 7, cation **15″** would form through the epoxidation of **14**, leading to the inverted
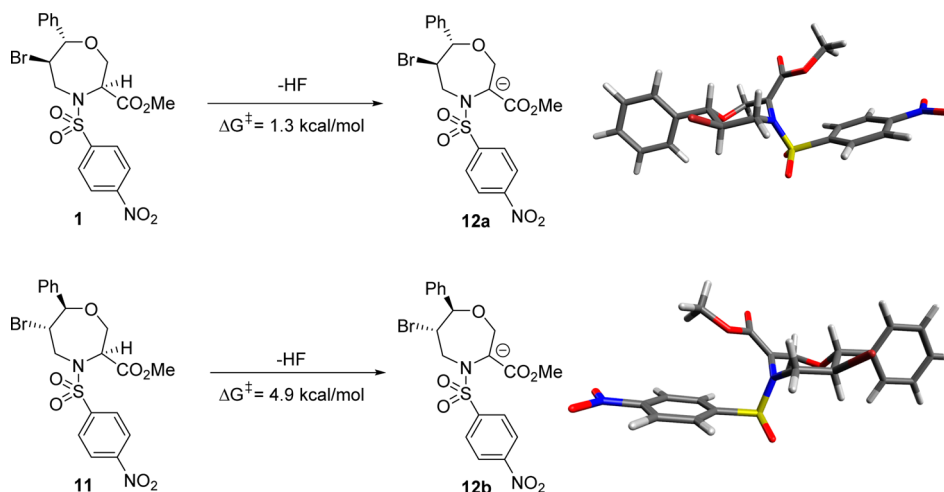

Figure 10. Loss of HF to produce intermediate enolates **12a** and **12b** from **1** and **11**, respectively.
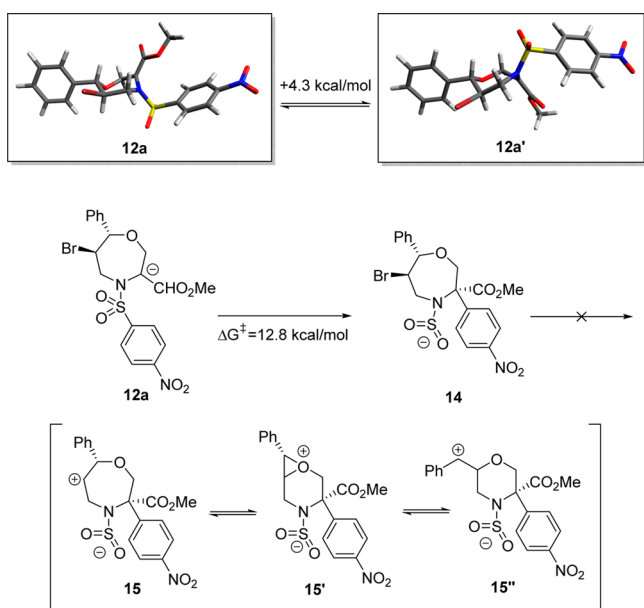
Figure 12. Investigation of alternative pathways leading to **2b**.

stereochemistry of the phenyl group. However, these structures were not stable: the optimizations led to ring opening or loss of SO_2 and high energies relative to **14** (see the Supporting Information for details). From the data obtained, it was clear that **12a**, when formed, can produce only one diastereoismer with no possible racemization during the course of the reaction. All other attempts to obtain **2b** suffered from high energies and unstable structures as well. Therefore, we believe that the ring

opening process shown in Figure 9 is responsible for the formation of product **2b**.

Overall, on the basis of the results obtained from the computational study, we propose that the mechanism to form **2a** starts with an enolate alkylation followed by the simultaneous loss of SO_2 and Br anion with the highly stereospecific formation of the aziridine. The mechanism of formation of **2b**, on the other hand, begins with a conformational change induced by a catalytic amount of HF, leading to **1′**, followed by an elimination/ring opening step and subsequent ring closure, allowing the inversion of the C6 and C7 substituents and the formation of **11**, a diastereomer of **1**. Compound **11** then follows the same mechanism as described above to produce **2b**. The two pathways have similar energies for their rate-determining step: taking compound **1′** as the lowest energy reference, the pathway starting with ring opening must overcome a barrier of 14.9 kcal/mol, whereas the pathway beginning with enolate alkylation requires 14.6 kcal/mol. The entire energy profile relative to **1** for these pathways is shown in Figure 13.

■ CONCLUSIONS

In summary, we have discovered a mild, environmentally friendly fluoride-mediated intramolecular rearrangement of 1,4-oxazepanes and morpholines featuring an enolizable proton in C3. This reaction created significant complexity in one step, including the generation of fused (**2**, **4d**, **4g**) and bridged (**4b**) ring systems in good conversions. We have presented a tentative mechanism supported by extensive computational data. We propose that the formation of **11**, a diastereomer of **1**, occurs through olefin intermediate **10**. Subsequent formation of
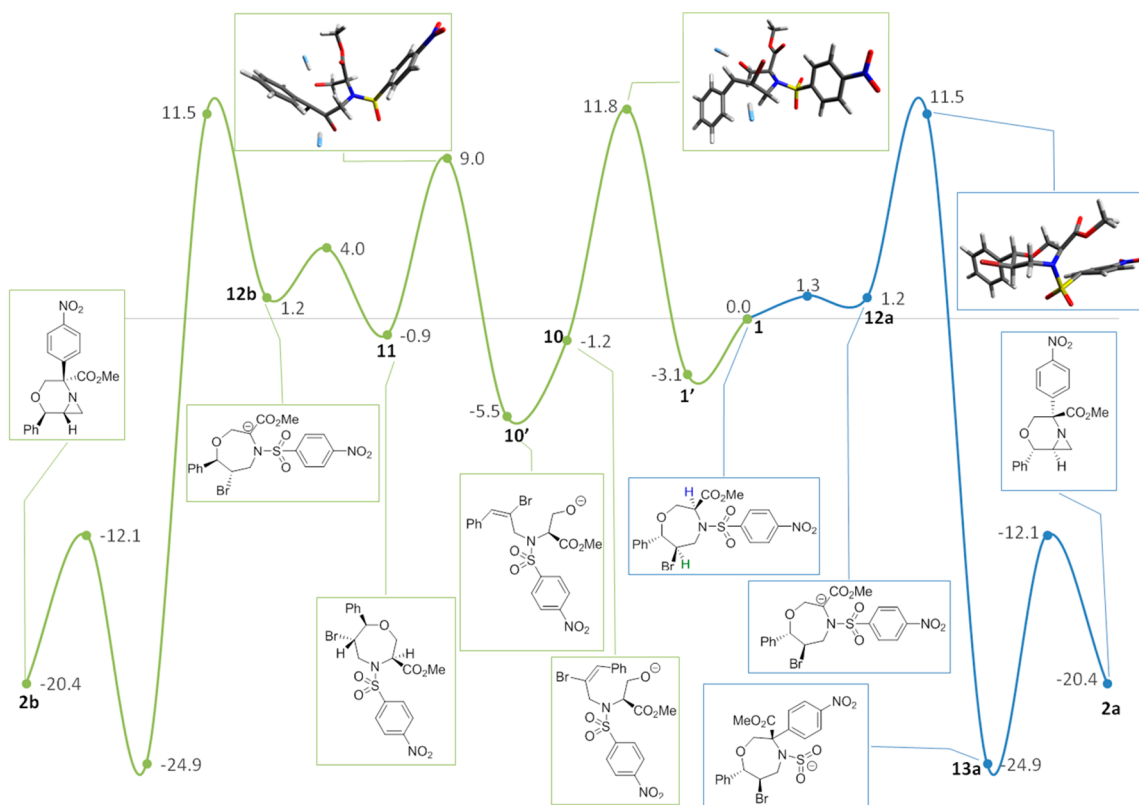

Figure 13. Overall energy profile (kcal/mol) for the reaction mechanism leading from **1** to **2a** (blue) and **2b** (green). Although HF, F, and Br anions and SO_2 were considered in the calculations of energies, they do not appear in the figure unless necessary to avoid overcrowding.

enantiomeric enolates from **1** and **11** is followed by migration of *para*-nitrophenyl, loss of SO$_2$, and ring contraction to give **2a** and **2b**, respectively. This mechanism is consistent with the experimental observations. At this stage, methods for increasing stereoselectivity are currently being evaluated in our lab and will be reported in due course.

■ EXPERIMENTAL SECTION

General Considerations. All commercially available reagents were used without further purification. All melting points are uncorrected. Chemical shifts (δ) are reported in parts per million (ppm) relative to CDCl$_3$ (7.26 ppm for ^{1}H and 77.160 ppm for ^{13}C). ^{1}H and ^{13}C NMR spectra were recorded at 400 or 500 and 100 or 125 MHz, respectively, and assignments were confirmed by 2D COSY, HSQC, HMQC, and NOESY experiments or by X-ray crystallography. Chromatography was performed on silica gel 60 (230−40 mesh). Visualization was performed by UV or by development using ceric ammonium molybdate, KMnO$_4$, or ninhydrin stains. Infrared spectra were recorded on an FT-IR spectrometer. HRMS were obtained by ESI-QTOF unless otherwise stated. Optical rotations were measured at the wavelength 589 nm (sodium D line). Compounds **1** and **3b–h** were made according to literature procedure.[15]

General Procedure for TBAF-Mediated Intramolecular Rearrangement of Oxazepanes and Morpholines. 1 (49 mg, 0.10 mmol) was dissolved in THF (4.5 mL). TBAF (1 M in THF, 500 μL, 0.50 mmol) was added, and the mixture immediately turned very dark. The mixture was stirred at rt for 1−16 h. The mixture was filtered through a Celite plug with THF and then concentrated under reduced pressure. The crude was purified by column chromatography (7:3 hexanes:EtOAc) or by semipreparative HPLC (95:5 H$_2$O:MeOH to 5:95 H$_2$O:MeOH, retention time 19.5 min, C14 Zorbax Bonus-RP column), and **2** was isolated as a white solid.

Methyl 2-(4-Nitrophenyl)-5-phenyl-4-oxa-1-azabicyclo[4.1.0]heptane-2-carboxylate (2). White solid; 38 mg isolated (46% yield, 36% ee); [α]$_D^{22}$ = +55.7° (*c* 1.90, CHCl$_3$); R$_f$ 0.16 (7:3 hexanes:EtOAc); mp 165−168 °C; IR (film, cm$^{−1}$) 2998, 2954, 2866, 1730, 1606, 1597, 1519, 1349, 1260, 1062, 856, 751, 740, 699; ^{1}H NMR (500 MHz, CDCl$_3$) δ 8.27 (d, *J* = 9.0 Hz, 2H), 7.89 (d, *J* = 9.0 Hz, 2H), 7.37−7.25 (m, 6H), 4.83 (d, *J* = 3.2 Hz, 1H), 4.01 (d, *J* = 12.9 Hz, 1H), 3.89 (d, *J* = 12.8 Hz, 1H), 3.80 (s, 3H), 2.68 (dt, *J* = 5.2, 3.5 Hz, 1H), 2.37 (d, *J* = 5.2 Hz, 1H), 2.09 (d, *J* = 3.6 Hz, 1H); ^{13}C NMR (125 MHz, CDCl$_3$) δ 171.3, 148.3, 147.5, 140.6, 128.8, 128.4, 127.5, 126.6, 123.7, 75.1, 64.8, 62.5, 53.2, 35.6, 30.9; HRMS: (M + Na) for C$_{19}$H$_{18}$O$_5$N$_2$Na calcd, 377.1113; found, 377.1111.

(1S,2S,5R)-Methyl 6-((4-nitrophenyl)sulfonyl)-2-phenyl-3-oxa-6-azabicyclo[3.2.0]heptane-5-carboxylate (2c). ^{1}H NMR (400 MHz, CDCl$_3$) δ 8.38 (d, *J* = 8.9 Hz, 2H), 8.12 (d, *J* = 8.9 Hz, 2H), 7.40−7.28 (m, 5H), 5.21 (s, 1H), 4.62 (d, *J* = 11.1 Hz, 1H), 4.18−4.10 (m, 2H), 4.07 (dd, *J* = 7.1, 4.4 Hz, 1H), 3.69 (s, 3H), 3.51 (dd, *J* = 7.2, 4.1 Hz, 1H), 3.36 (m, 6.6 Hz, 1H).

(3S,6R,7S)-Methyl 6-Iodo-4-((4-nitrophenyl)sulfonyl)-7-phenyl-1,4-oxazepane-3-carboxylate (3a). Colorless oil; 60 mg isolated (46% yield); [α]$_D^{22}$ = +8.2° (*c* 1.20, CHCl$_3$); R$_f$ 0.65 (CH$_2$Cl$_2$); IR (film, cm$^{−1}$) 3105, 3066, 3035, 2955, 2882, 1745, 1530, 1349, 1160, 1094, 1019, 1011, 890, 855, 777, 759, 745, 735, 700; ^{1}H NMR (400 MHz, CDCl$_3$) δ 8.40 (d, *J* = 8.9 Hz, 2H), 8.08 (d, *J* = 8.9 Hz, 2H), 7.35 (dd, *J* = 5.2, 1.9 Hz, 3H), 7.28 (d, *J* = 3.1 Hz, 2H), 5.07 (dd, *J* = 10.1, 7.1 Hz, 1H), 4.56−4.48 (m, 2H), 4.34 (ddd, *J* = 10.6, 9.9, 3.2 Hz, 2H), 3.75 (ddd, *J* = 17.2, 14.9, 11.4 Hz, 2H), 3.64 (s, 3H); ^{13}C NMR (100 MHz, CDCl$_3$) δ 169.3, 150.2, 145.5, 138.8, 129.0, 128.7, 128.5, 127.4, 124.4, 92.1, 69.4, 59.5, 52.7, 52.1, 32.0; HRMS: (M + Na) for C$_{19}$H$_{19}$IN$_2$O$_7$SNa calcd, 568.9855; found, 568.9851.

(3S,6S,7R)-Methyl 6-Iodo-4-((4-nitrophenyl)sulfonyl)-7-phenyl-1,4-oxazepane-3-carboxylate (3a′). White solid; 14 mg isolated (11% yield); mp 211−215 °C; [α]$_D^{22}$ = −87.6° (*c* 0.43, CH$_2$Cl$_2$); R$_f$ 0.54 (CH$_2$Cl$_2$); IR (film, cm$^{−1}$) 3105, 3066, 3035, 2953, 2871, 1747, 1530, 1349, 1164, 1091, 855, 759, 744, 735, 700, 686; ^{1}H NMR (500 MHz, CDCl$_3$) δ 8.39 (d, *J* = 9.0 Hz, 2H), 8.09 (d, *J* = 9.0 Hz, 2H), 7.37−7.29 (m, 3H), 7.26−7.21 (m, 2H), 4.80−4.75 (m, 2H),

4.58 (dd, *J* = 13.5, 2.7 Hz, 1H), 4.46−4.40 (m, 1H), 4.32 (dd, *J* = 15.5, 2.6 Hz, 1H), 4.17 (dd, *J* = 13.5, 2.6 Hz, 1H), 3.99 (dd, *J* = 15.3, 7.6 Hz, 1H), 3.73 (s, 3H); ^{13}C NMR (125 MHz, CDCl$_3$) δ 169.6, 150.3, 145.0, 140.3, 129.0, 128.8, 128.6, 126.6, 124.3, 90.1, 69.8, 61.7, 52.9, 52.3, 32.5; HRMS: (M + Na) for C$_{19}$H$_{19}$IN$_2$O$_7$SNa calcd, 568.9855; found, 568.9848.

(1R,3R,4R)-Methyl 1,3-Dimethyl-5-((4-nitrophenyl)sulfonyl)-2-oxa-5-azabicyclo[2.2.1]heptane-4-carboxylate (4b). Colorless oil; 10 mg isolated (27% yield); [α]$_D^{22}$ = −0.96° (*c* 0.50, CHCl$_3$); R$_f$ 0.31 (7:3 hexanes:EtOAc); IR (film, cm$^{−1}$) 3107, 2957, 1745, 1529, 1349, 1166, 1144, 1098, 1077, 855, 687; ^{1}H NMR (400 MHz, CDCl$_3$) δ 8.35 (d, *J* = 9.0 Hz, 2H), 8.11 (d, *J* = 9.0 Hz, 2H), 4.54 (q, *J* = 6.2 Hz, 1H), 3.84 (s, 3H), 3.59 (dd, *J* = 8.3, 1.5 Hz, 1H), 3.17 (d, *J* = 8.3 Hz, 1H), 2.28 (dd, *J* = 9.9, 1.5 Hz, 1H), 2.14 (d, *J* = 9.9 Hz, 1H), 1.53 (d, *J* = 6.2 Hz, 3H), 1.40 (s, 3H); ^{13}C NMR (125 MHz, CDCl$_3$) δ 199.0, 163.9, 147.6, 130.3, 128.8, 123.1, 122.8, 96.8, 52.3, 28.5, 12.8; HRMS: (M + Na) for C$_{15}$H$_{18}$N$_2$O$_7$SNa calcd, 393.0732; found, 393.0730.

4-((4-Nitrophenyl)sulfonyl)-7-phenyl-2,3,4,7-tetrahydro-1,4-oxazepine (4c). Yellow oil; 6 mg isolated (25% yield); R$_f$ 0.65 (7:3 hexanes:EtOAc); IR (film, cm$^{−1}$) 3293, 3106, 2928, 2872, 1720, 1529, 1349,1310, 1166, 1107, 1091, 855, 737; ^{1}H NMR (500 MHz, CDCl$_3$) δ 8.41 (d, *J* = 9.0 Hz, 2H), 8.05 (d, *J* = 9.0 Hz, 2H), 7.37−7.27 (m, 3H), 7.25−7.21 (m, 2H), 6.67 (dd, *J* = 9.8, 2.0 Hz, 1H), 5.18−5.15 (m, 1H), 5.12 (dd, *J* = 9.8, 3.2 Hz, 1H), 4.03−3.93 (m, 2H), 3.69 (ddd, *J* = 9.6, 7.9, 3.0 Hz, 1H), 3.60−3.51 (m, 1H); ^{13}C NMR (125 MHz, CDCl$_3$) δ 150.4, 144.2, 140.4, 128.6, 128.3, 128.2, 126.9, 126.6, 124.6, 116.8, 79.9, 67.0, 51.7; HRMS (APCI): (M + H) for C$_{17}$H$_{17}$N$_2$O$_5$S calcd, 361.0853; found, 361.0848.

(2S,3R,6S)-Methyl 3,5,5-Trimethyl-2-(4-nitrophenyl)-4-oxa-1-azabicyclo[4.1.0]heptane-2-carboxylate (4d). Colorless oil; 42 mg isolated (61% yield); [α]$_D^{22}$ = +96.1° (*c* 0.84, CHCl$_3$); R$_f$ 0.14 (7:3 hexanes:EtOAc); IR (film, cm$^{−1}$) 2979, 1732, 1520, 1345, 1256, 1074, 1050, 852, 709; ^{1}H NMR (400 MHz, CDCl$_3$) δ 8.22 (d, *J* = 8.9 Hz, 2H), 7.51 (d, *J* = 8.9 Hz, 2H), 3.94 (q, *J* = 6.2 Hz, 1H), 3.81 (s, 3H), 2.54 (dd, *J* = 5.6, 4.4 Hz, 1H), 1.93 (m, 2H), 1.53 (s, 3H), 1.30 (s, 3H), 0.96 (d, *J* = 6.2 Hz, 3H); ^{13}C NMR (125 MHz, CDCl$_3$) δ 171.9, 147.1, 145.6, 129.2, 122.5, 68.4, 66.5, 62.2, 52.9, 41.2, 31.8, 26.8, 25.0, 18.3; HRMS: (M + Na) for C$_{16}$H$_{20}$N$_2$O$_5$Na calcd, 343.1270; found, 343.1264.

(1S,2S,4R,5R)-Methyl 4-Methyl-6-((4-nitrophenyl)sulfonyl)-2-phenyl-3-oxa-6-azabicyclo[3.2.0]heptane-5-carboxylate (4fa). Colorless crystalline solid; 1 mg isolated (<1% yield); [α]$_D^{22}$ = 18.8° (*c* 1.05, CHCl$_3$); R$_f$ 0.36 (7:3 hexanes:EtOAc); mp 175−181 °C; IR (film, cm$^{−1}$) 2962, 2877, 1740, 1530, 1350, 1275, 1164, 1108, 855, 738; ^{1}H NMR (400 MHz, CDCl$_3$) δ 8.39 (d, *J* = 8.9 Hz, 2H), 8.04 (d, *J* = 8.9 Hz, 2H), 7.35 (dd, *J* = 8.0, 6.5 Hz, 2H), 7.29 (d, *J* = 7.2 Hz, 1H), 7.23 (d, *J* = 7.6 Hz, 2H), 5.16 (s, 1H), 4.54 (dd, *J* = 8.6, 7.1 Hz, 1H), 4.36 (q, *J* = 6.1 Hz, 1H), 3.85 (dd, *J* = 7.1, 3.7 Hz, 1H), 3.83 (s, 3H), 3.53 (dd, *J* = 8.6, 3.7 Hz, 1H), 1.37 (d, *J* = 6.1 Hz, 3H); ^{13}C NMR (125 MHz, CDCl$_3$) δ 168.3, 150.1, 145.7, 139.4, 128.8, 128.3, 128.0, 125.7, 124.3, 84.4, 82.6, 76.2, 54.1, 53.1, 45.1, 14.5; HRMS: (M + Na) for C$_{20}$H$_{20}$N$_2$O$_7$SNa calcd, 455.0889; found, 455.0886.

(2S,3R,5R,6R)-Methyl 3-Methyl-2-(4-nitrophenyl)-5-phenyl-4-oxa-1-azabicyclo[4.1.0]heptane-2-carboxylate (4fb). Colorless oil; 56 mg isolated (14% yield); R$_f$ 0.19 (7:3 hexanes:EtOAc); IR (film, cm$^{−1}$) 2951, 1741, 1521, 1349, 1220; ^{1}H NMR (400 MHz, CDCl$_3$) δ 8.18 (d, *J* = 9.0 Hz, 2H), 7.62 (d, *J* = 9.0 Hz, 2H), 7.55 (m, 2H), 7.41 (m, 2H), 7.33 (m, 1H), 5.45 (s, 1H), 3.84 (s, 3H), 3.33 (q, *J* = 6.7 Hz, 1H), 3.00 (dd, *J* = 5.2, 4.0 Hz, 1H), 2.32 (d, *J* = 5.2 Hz, 1H), 2.21 (d, *J* = 4.0 Hz, 1H), 1.27 (d, *J* = 6.7 Hz, 3H); ^{13}C NMR (100 MHz, CDCl$_3$) δ 170.0, 149.6, 147.1, 139.2, 128.8, 128.2, 128.2, 127.4, 123.2, 72.1, 70.7, 67.8, 52.4, 32.5, 30.0 15.7; HRMS: (M + Na) for C$_{20}$H$_{20}$N$_2$O$_5$Na calcd, 391.1270; found, 391.1269.

(2S,3R,5S,6S)-Methyl 3-Methyl-2-(4-nitrophenyl)-5-phenyl-4-oxa-1-azabicyclo[4.1.0]heptane-2-carboxylate (4fc). Colorless oil; 4 mg isolated (1% yield); [α]$_D^{22}$ = +298.8° (*c* 0.85, CHCl$_3$); R$_f$ 0.15 (7:3 hexanes:EtOAc); IR (film, cm$^{−1}$) 2952, 17.32, 1606, 1519, 1345, 1254, 1220, 1112, 1065, 1038, 853, 740; ^{1}H NMR (400 MHz, CDCl$_3$) δ 8.25 (d, *J* = 8.9 Hz, 2H), 7.58 (d, *J* = 8.9 Hz, 2H), 7.47−7.32 (m,

5H), 4.84 (d, J = 4.7 Hz, 1H), 3.95 (q, J = 6.2 Hz, 1H), 3.87 (s, 3H), 2.76 (td, J = 4.7, 3.5 Hz, 1H), 2.25 (d, J = 5.2 Hz, 1H), 2.07 (d, J = 3.5 Hz, 1H), 1.05 (d, J = 6.2 Hz, 3H); ^{13}C NMR (125 MHz, CDCl$_3$) δ 171.7, 147.2, 145.8, 141.3, 129.1, 128.9, 128.2, 125.8, 122.6, 77.1, 69.2, 65.7, 53.0, 38.0, 30.9, 18.2; HRMS: (M + H) for C$_{20}$H$_{21}$N$_2$O$_5$ calcd, 369.1445; found, 369.1454.

Methyl 4-Hydroxy-1-((4-nitrophenyl)sulfonyl)-3-phenyl-2-vinylpyrrolidine-2-carboxylate (4fd). Characterized as a 1:1 mixture of diastereomers: yellow oil; 44 mg isolated (11% yield); R_f 0.56 (7:3 hexanes/EtOAc); IR (film, cm^{-1}) 2953, 1733, 1605, 1519, 1236, 854, 751, 698; ^{1}H NMR (500 MHz, CDCl$_3$) δ 8.20 (d, J = 8.7 Hz, 2H), 7.64 (m, 2H), 7.39−7.29 (m, 3H), 7.25−7.22 (m, 2H), 6.30 (m, 1H), 5.50−5.41 (m, 2H), 3.82 (m, 1H), 3.77 (s, 3H), 3.19−3.14 (m, 1H), 2.87 (m, 1H), 2.65 (m, 1H); ^{13}C NMR (125 MHz, CDCl$_3$) δ 172.6, 147.8, 147.3, 136.9, 136.5, 136.5, 128.5, 128.3, 128.2, 128.1, 125.6, 125.6, 123.6, 118.1, 118.0, 69.8, 69.7, 62.1, 62.0, 56.9, 56.7, 52.9, 45.1, 44.8; HRMS: (M + Na) for C$_{20}$H$_{20}$N$_2$O$_5$Na calcd, 391.1270; found, 391.1274.

(2R,3S,5R,6R)-Methyl 3-Methyl-2-(4-nitrophenyl)-5-phenyl-4-oxa-1-azabicyclo[4.1.0]heptane-2-carboxylate (4g). Colorless oil; 87 mg isolated (69% yield); $[\alpha]_D^{22}$ = 53.4° (c 4.35, CHCl$_3$); R_f 0.16 (7:3 hexanes:EtOAc); IR (film, cm^{-1}) 2950, 2898, 1739, 1519, 1347, 1239, 1037, 999, 853, 753; ^{1}H NMR (500 MHz, CDCl$_3$) δ 8.18 (d, J = 9.0 Hz, 2H), 7.62 (d, J = 9.0 Hz, 2H), 7.54 (d, J = 7.4 Hz, 2H), 7.41 (t, J = 7.6 Hz, 2H), 7.33 (t, J = 7.4 Hz, 1H), 5.44 (s, 1H), 3.83 (s, 3H), 3.33 (q, J = 6.7 Hz, 1H), 2.99 (dd, J = 5.0, 4.1 Hz, 1H), 2.31 (d, J = 5.3 Hz, 1H), 2.21 (d, J = 3.9 Hz, 1H), 1.26 (d, J = 6.7 Hz, 3H); ^{13}C NMR (125 MHz, CDCl$_3$) δ 170.0, 149.6, 147.1, 139.2, 128.8, 128.2, 128.2, 127.4, 123.2, 72.1, 70.7, 67.8, 52.4, 32.5, 30.0, 15.7; HRMS: (M + H) for C$_{20}$H$_{21}$N$_2$O$_5$ calcd, 369.1445; found, 369.1451.

(2R,3S,5S,6S)-Methyl 3-Methyl-2-(4-nitrophenyl)-5-phenyl-4-oxa-1-azabicyclo[4.1.0]heptane-2-carboxylate (4hb). $[\alpha]_D^{22}$ = −12.7° (c 0.30, CHCl$_3$); ^{1}H NMR (400 MHz, CDCl$_3$) δ 8.18 (d, J = 9.0 Hz, 2H), 7.62 (d, J = 9.0 Hz, 2H), 7.55 (m, 2H), 7.41 (m, 2H), 7.33 (m, 1H), 5.45 (s, 1H), 3.84 (s, 3H), 3.33 (q, J = 6.7 Hz, 1H), 3.00 (dd, J = 5.2, 4.0 Hz, 1H), 2.32 (d, J = 5.2 Hz, 1H), 2.21 (d, J = 4.0 Hz, 1H), 1.27 (d, J = 6.7 Hz, 3H).

(+)-Methyl 6-Methyl-2-(4-nitrophenyl)-5-phenyl-4-oxa-1-azabicyclo[4.1.0]heptane-2-carboxylate (4i). Colorless oil; 3 mg isolated yield (21%); $[\alpha]_D^{22}$ = 274° (c 0.15, CH$_2$Cl$_2$); R_f 0.20 (70:30 hexanes:EtOAc); IR (film, cm^{-1}) 2956, 1730, 1520, 1350, 1271, 1243, 1100, 1067, 1027, 857, 702; ^{1}H NMR (400 MHz, CDCl$_3$) δ 8.31 (d, J = 9.0 Hz, 2H), 7.87 (d, J = 9.0 Hz, 2H), 7.29 (m, 3H), 7.15 (m, 2H), 4.87 (s, 1H), 4.04 (d, J = 12.8 Hz, 1H), 3.94 (d, J = 12.8 Hz, 1H), 3.80 (s, 3H), 2.20 (s, 1H), 2.09 (s, 1H), 1.55 (s, 1H), 1.06 (s, 3H); ^{13}C NMR (100 MHz, CDCl$_3$) δ 171.4, 148.7, 147.5, 138.4, 128.3, 127.8, 127.5, 123.7, 79.2, 65.5, 63.7, 53.2, 38.2, 37.9, 23.8; HRMS: (M + Na) for C$_{20}$H$_{20}$N$_2$O$_5$Na calcd, 391.1270; found, 391.1276.

(2S,3R,5S)-Methyl 3,5-Dimethyl-2-(4-nitrophenyl)-4-oxa-1-azabicyclo[4.1.0]heptane-2-carboxylate (4j). Colorless oil; 9 mg isolated yield (22%); $[\alpha]_D^{22}$ = 110° (c 0.45, CH$_2$Cl$_2$); R_f 0.06 (70:30 hexanes:EtOAc); IR (film, cm^{-1}) 2980, 1732, 1520, 1346, 1256, 1077, 1048, 853, 710; ^{1}H NMR (400 MHz, CDCl$_3$) δ 8.21 (d, J = 8.9 Hz, 2H), 7.48 (d, J = 8.9 Hz, 2H), 3.96−3.88 (m, 1H), 3.84 (s, 3H), 3.74 (q, J = 6.3 Hz, 1H), 2.47 (dd, J = 8.9, 4.2 Hz, 1H), 2.13 (d, J = 5.2 Hz, 1H), 1.86 (d, J = 3.6 Hz, 1H), 1.51 (d, J = 6.4 Hz, 3H), 0.94 (d, J = 6.3 Hz, 3H); ^{13}C NMR (100 MHz, CDCl$_3$) δ 171.2, 147.1, 145.9, 129.1, 122.6, 71.1, 68.9 66.0, 52.9, 37.7, 30.4, 22.3, 18.9; HRMS: (M + Na) for C$_{15}$H$_{18}$N$_2$O$_5$Na calcd, 329.1113; found, 329.1113.

Molecular Modeling. All calculations were performed using ORCA 3.0.1[20] ab initio software. The structures were obtained by B3LYP/def2-SVP and recomputed to get single-point energies at the def2-TZVP level. An implicit solvent model COSMO was used to take the influence of THF into account. The molecular orbitals, frequencies, and structures were visualized using Avogadro[21] and Iboview.[22]

X-ray Crystallography. Crystal and molecular structures of **2** and **4fa** were determined by single-crystal X-ray diffraction. Diffraction measurements were made on a Bruker D8 APEX2 X-ray diffractometer instrument using graphite-monochromated Mo Kα (λ = 0.71073 Å)

radiation. The X-ray diffraction data sets were collected using the ω scan mode over the 2θ range up to 54°. The structures were solved by direct methods implemented in SHELXS and refined using SHELXL.[23] Structure refinement was performed on F^2 using all data, and hydrogen atoms were located from the electron difference map whenever data quality was sufficient. Otherwise, hydrogen atoms on carbon centers were modeled with appropriate riding-hydrogen models. Calculations were performed and the drawings were prepared using the WINGX[24] suite of crystallographic programs. Compound **2** crystallizes in centrosymmetric space group $P2_1/n$ and is not enantiopure. Compound **4fa** crystallizes in enantiomorphic space group $P2_12_12_1$. The absolute configuration of **4fa** was determined from anomalous scattering, with the Flack parameter of 0.04(3). Structures have been deposited with the Cambridge Structural Database (deposition codes 1429192 and 1429193).

■ ASSOCIATED CONTENT

Ⓢ Supporting Information

The Supporting Information is available free of charge on the ACS Publications website at DOI: 10.1021/acs.joc.6b02999.

> Spectroscopic data for all new compounds (PDF)
> Chiral HPLC chromatograms, energy data, and structures from theoretical calculations (PDF)
> X-ray crystallographic data for **2** (CIF)
> X-ray crystallographic data for **4fa** (CIF)

■ AUTHOR INFORMATION

Corresponding Author

*E-mail: nicolas.moitessier@mcgill.ca.

ORCID ⬤

Nicolas Moitessier: 0000-0001-6933-2079

Notes

The authors declare no competing financial interest.

■ REFERENCES

(1) Schreiber, S. L. *Science* **2000**, *287*, 1964.
(2) Burke, M. D.; Schreiber, S. L. *Angew. Chem., Int. Ed.* **2004**, *43*, 46.
(3) Padwa, A. *Chem. Soc. Rev.* **2009**, *38*, 3072.
(4) Shi, M.; Wu, L.; Lu, J. M. *J. Org. Chem.* **2008**, *73*, 8344.
(5) Yao, L. F.; Wei, Y.; Shi, M. *J. Org. Chem.* **2009**, *74*, 9466.
(6) Sun, Y. W.; Tang, X. Y.; Shi, M. *Chem. Commun.* **2015**, *51*, 13937.
(7) Brook, A. G. *Acc. Chem. Res.* **1974**, *7*, 77.
(8) Meier, H.; Zeller, K.-P. *Angew. Chem., Int. Ed. Engl.* **1975**, *14*, 32.
(9) Sibi, M. P.; Snieckus, V. *J. Org. Chem.* **1983**, *48*, 1935.
(10) Riggs, J. C.; Singh, K. J.; Yun, M.; Collum, D. B. *J. Am. Chem. Soc.* **2008**, *130*, 13709.
(11) Ilyin, A.; Kysil, V.; Krasavin, M.; Kurashvili, I.; Ivachtchenko, A. V. *J. Org. Chem.* **2006**, *71*, 9544.
(12) Kumar, N. N. B.; Kuznetsov, D. M.; Kutateladze, A. G. *Org. Lett.* **2015**, *17*, 438.
(13) Huot, M.; Moitessier, N. *Tetrahedron Lett.* **2010**, *51*, 2820.
(14) Moitessier, N.; Henry, C.; Aubert, N.; Chapleur, Y. *Tetrahedron Lett.* **2005**, *46*, 6191.
(15) Bezanson, M.; Pottel, J.; Bilbeisi, R.; Toumieux, S.; Cueto, M.; Moitessier, N. *J. Org. Chem.* **2013**, *78*, 872.
(16) Charrier, J.-D.; Hadfield, D. S.; Hitchcock, P. B.; Young, D. W. *Org. Biomol. Chem.* **2004**, *2*, 474.

(17) Duttagupta, I.; Goswami, K.; Sinha, S. *Tetrahedron* **2012**, *68*, 8347.

(18) Patonay, T.; Hegedus, L.; Patonay-Peli, E. *J. Heterocycl. Chem.* **1993**, *30*, 145.

(19) Foschi, F.; Landini, D.; Lupi, V.; Mihali, V.; Penso, M.; Pilati, T.; Tagliabue, A. *Chem. - Eur. J.* **2010**, *16*, 10667.

(20) Neese, F. *WIREs Comput. Mol. Sci.* **2012**, *2*, 73.

(21) *Avogadro*: an open-source molecular builder and visualization tool, version 1.1.1. http://avogadro.cc/

(22) Knizia, G.; Klein, J. E. M. N. *Angew. Chem., Int. Ed.* **2015**, *54*, 5518.

(23) Sheldrick, G. M. *Acta Crystallogr., Sect. A: Found. Crystallogr.* **2008**, *64*, 112.

(24) Farrugia, L. *J. Appl. Crystallogr.* **1999**, *32*, 837.